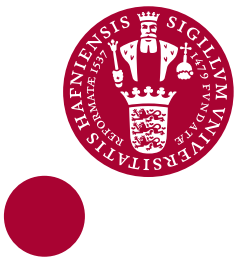

Climate data induced uncertainty in model-based estimations of terrestrial primary productivity

Wu, Zhendong; Ahlstrom, Anders; Smith, Benjamin; Ardö, Jonas; Eklundh, Lars; Fensholt, Rasmus; Lehsten, Veiko

Published in:
Environmental Research Letters

DOI:
10.1088/1748-9326/aa6fd8

Publication date:
2017

Document version
Publisher's PDF, also known as Version of record

Climate data induced uncertainty in model-based estimations of terrestrial primary productivity

Environmental Research Letters

LETTER

Climate data induced uncertainty in model-based estimations of terrestrial primary productivity

Zhendong Wu[1,2,5], Anders Ahlström[1,3], Benjamin Smith[1], Jonas Ardö[1], Lars Eklundh[1], Rasmus Fensholt[2] and Veiko Lehsten[1,4]

[1] Department of Physical Geography and Ecosystem Science, Lund University, Sölvegatan 12, SE-223 62 Lund, Sweden
[2] Department of Geosciences and Natural Resource Management, University of Copenhagen, 1350 Copenhagen, Denmark
[3] Department of Earth System Science, School of Earth, Energy and Environmental Sciences, Stanford University, Stanford, CA 94305, United States of America
[4] Swiss Federal Institute for Forest, Snow and Landscape research (WSL), Zürcherstr. 11 CH-8903, Birmensdorf, Switzerland
[5] Author to whom any correspondence should be addressed.

E-mail: zhendong.wu@nateko.lu.se

Keywords: climate datasets, GPP, uncertainty, LPJ-GUESS, apparent model sensitivity, climate data range, global carbon cycle

Supplementary material for this article is available online

OPEN ACCESS

RECEIVED
1 September 2016

REVISED
23 April 2017

ACCEPTED FOR PUBLICATION
27 April 2017

PUBLISHED
13 June 2017

Abstract

Model-based estimations of historical fluxes and pools of the terrestrial biosphere differ substantially. These differences arise not only from differences between models but also from differences in the environmental and climatic data used as input to the models. Here we investigate the role of uncertainties in historical climate data by performing simulations of terrestrial gross primary productivity (GPP) using a process-based dynamic vegetation model (LPJ-GUESS) forced by six different climate datasets. We find that the climate induced uncertainty, defined as the range among historical simulations in GPP when forcing the model with the different climate datasets, can be as high as 11 Pg C yr^{-1} globally (9% of mean GPP). We also assessed a hypothetical maximum climate data induced uncertainty by combining climate variables from different datasets, which resulted in significantly larger uncertainties of 41 Pg C yr^{-1} globally or 32% of mean GPP. The uncertainty is partitioned into components associated to the three main climatic drivers, temperature, precipitation, and shortwave radiation. Additionally, we illustrate how the uncertainty due to a given climate driver depends both on the magnitude of the forcing data uncertainty (climate data range) and the apparent sensitivity of the modeled GPP to the driver (apparent model sensitivity). We find that LPJ-GUESS overestimates GPP compared to empirically based GPP data product in all land cover classes except for tropical forests. Tropical forests emerge as a disproportionate source of uncertainty in GPP estimation both in the simulations and empirical data products. The tropical forest uncertainty is most strongly associated with shortwave radiation and precipitation forcing, of which climate data range contributes higher to overall uncertainty than apparent model sensitivity to forcing. Globally, precipitation dominates the climate induced uncertainty over nearly half of the vegetated land area, which is mainly due to climate data range and less so due to the apparent model sensitivity. Overall, climate data ranges are found to contribute more to the climate induced uncertainty than apparent model sensitivity to forcing. Our study highlights the need to better constrain tropical climate, and demonstrates that uncertainty caused by climatic forcing data must be considered when comparing and evaluating carbon cycle model results and empirical datasets.

1. Introduction

The climate affects a multitude of vegetation processes, resulting in complex and variable interactions (Luo 2007, Luo *et al* 2008, Zhou *et al* 2008). Dynamic Global Vegetation Models (DGVMs) attempt to describe such complexity using globally-applicable representation of vegetation structure and composition, ecosystem biogeochemistry and the responses of underlying physiological and ecological processes to variations in climate, atmospheric CO_2 and other drivers (Prentice *et al* 2007, Scheiter *et al* 2013). DGVMs integrate available knowledge of ecological processes by combining theoretical process understanding with data from laboratory studies, field measurements and satellite-based estimations, and apply this knowledge to simulate ecosystem functions, such as carbon uptake and cycling, normally across a grid spanning the global land area. DGVMs complement observation-based methods such as remote sensing and field measurements by explicitly accounting for the process interactions and feedbacks linking climate and other forcings to ecosystem dynamics. They are widely used in global change impact and process studies, for characterisation of the terrestrial carbon cycle and its responses to greenhouse gas emissions and climate change, and as a component in Earth system models, accounting for biogeochemical and biophysical biosphere-atmosphere feedbacks (Scholze *et al* 2006, Hickler *et al* 2008, Sitch *et al* 2008, Sitch *et al* 2015). Gross Primary Production (GPP), the total amount of carbon assimilated by plants via photosynthesis, is a fundamental driver of vegetation processes, playing an important role in the global carbon cycle (Cox and Jones 1993, Battin *et al* 2009). It is a fundamental process simulated by all DGVMs. Many models adopt one of the available variants of the Farquhar *et al* (1980) biochemical photosynthesis model. In DGVMs, GPP represents the origin of carbon within the simulated ecosystem, controlling many other downstream processes. If GPP is simulated incorrectly, errors propagate to other processes and affect all carbon pools and fluxes of the simulated ecosystem (Luo *et al* 2003).

Although GPP is a fundamental flux of the carbon cycle, observation-based estimates of global GPP differ significantly between products based on remote sensing (Earth-Observation, EO-based), flux towers or a combination thereof. GPP estimates also differ between DGVMs and between DGVMs and observation-based datasets (Jung *et al* 2007, Jung *et al* 2011, Piao *et al* 2013, Anav *et al* 2015, Sitch *et al* 2015). Some of the discrepancies between GPP estimates of different DGVMs originate from model structural uncertainty arising from different representations of the same ecological processes, the scaling of these processes, their interactions and linkages to drivers and descriptors of ecosystem state, as well as the inclusion of certain processes, e.g. wildfires or nutrient interactions, in some models but not others (Cramer *et al* 2001, Gurney *et al* 2004, Tebaldi and Knutti 2007, Sitch *et al* 2008, De Kauwe *et al* 2014, Zaehle *et al* 2014). Additional uncertainty stems from parameter uncertainty due to different model calibration strategies (Knorr and Heimann 2001, Zaehle *et al* 2005, Wramneby *et al* 2008). In both DGVMs as well as models based on empirical data further uncertainty propagates from the environmental driver data, particularly data on climate variables such as temperature, precipitation, solar insolation, wind speed and atmospheric humidity, used to force or extrapolate the models (McGuire *et al* 2001, Zhao *et al* 2006, Jung *et al* 2007, Poulter *et al* 2011, Ahlström *et al* 2012b, Ahlström *et al* 2013). The climate inputs used in DGVMs are derived from either quasi-point-based measurements or model-based reanalyses. These variables need to be interpolated across areas of unmeasured territory to supply a model with values at each grid cell for the simulation, which inevitably introduces uncertainty propagating through the ecosystem model (Zhao *et al* 2006). A thorough and strict quantification of climate induced uncertainties is required to provide a robust interpretation and quantification of output from DGVM simulations. At present, little is known about how much each climate variable contributes to total climate induced uncertainty in GPP, and no studies have to our knowledge partitioned the uncertainty into components associated with climate data range (the magnitude of the forcing data uncertainty) and apparent sensitivity of the model to each individual driver of GPP.

Here we employ an individual-based DGVM (LPJ-GUESS) previously applied in a wide range of carbon cycle and climate impact studies to assess and quantify the potential uncertainty of estimated terrestrial GPP caused by climate driver uncertainty. We apply six historical climate datasets as input to simulations of the global terrestrial carbon cycle, and partition the revealed uncertainty into components propagating from different climatic drivers, in terms of forcing data range and the apparent sensitivity of the simulated ecosystem response to forcing, globally and among major bioclimatic regions.

2. Methodology

2.1. DGVM

We employ the Lund-Potsdam-Jena General Ecosystem Simulator (LPJ-GUESS; Smith *et al* 2001, Smith *et al* 2014) to estimate GPP. LPJ-GUESS is a DGVM which uniquely combines an individual-based representation of woody plant growth, demography and interspecific competition with process-based physiology and biogeochemistry. It employs gridded time series of climate data (air temperature, precipitation and incoming shortwave radiation) as forcing and

Table 1. Description and source of climate datasets used in the analysis.

Dataset	Spatial resolution	Time period	References
CRU TS 3.21	0.5 degree	1901–2012	Jones and Harris (2013)
CRUNCEP v5	0.5 degree	1901–2013	Wei *et al* (2013)
ECMWF/ERA Interim	0.5 degree	1979–2014	Dee *et al* (2011)
NCEP-DOE II	2.5 degree	1979–2014	Kanamitsu *et al* (2002)
PRINCETON_V2	0.5 degree	1901–2012	Sheffield *et al* (2006)
WFDEI_GPCC	0.5 degree	1979–2010	Weedon *et al* (2011)

simulates the effects of climate on vegetation structure and composition in terms of plant functional types (PFTs), soil hydrology and biogeochemistry. Atmospheric carbon dioxide (CO_2) concentrations, nitrogen (N) deposition rates and soil physical properties (fixed) provide additional inputs. The 11 PFTs adopted for the present study and their prescribed parameters are given in tables S1 and S2 available at stacks.iop.org/ERL/12/064013/mmedia. We employ LPJ-GUESS version 3.0 which incorporates ecosystem nitrogen cycling, and the CENTURY soil biogeochemistry scheme (Parton *et al* 1993). A full description of the LPJ-GUESS is given in Smith *et al* (2014) and references therein.

2.1.1. Simulations

LPJ-GUESS is forced with six alternative climate datasets (each including temperature, precipitation and shortwave radiation (table 1)) in separate simulations. To ensure comparability, all climate datasets are regridded to a 0.5 × 0.5 degrees spatial resolution, aggregated to a monthly temporal resolution. These monthly datasets are interpolated to daily values uniformly within LPJ-GUESS according to Gerten *et al* (2004). The CRU dataset is derived from climate station records and constructed using the Climate Anomaly Method, CAM (Peterson *et al* 1998). CRU and CRUNCEP differ mainly in shortwave radiation where CRUNCEP calculate radiation transfer differently (Wei *et al* 2013) from the method applied within LPJ-GUESS to data on cloud cover. NCEP and ECMWF are reanalysis data, which are generated by combining observations with a meteorological forecast model. The other two datasets (WFDEI and PRINCETON) are hybrid datasets combining observations and reanalysis data.

Simulations are initialized with a 500 year spin-up where the model is forced by re-cycled de-trended 1979–2010 climate data, to achieve vegetation and soil carbon pools in equilibrium with the forcing climate. 500 years is sufficient to establish vegetation and litter inputs to the soil which in conjunction with respiration rates are used to solve the slower soil carbon pools steady state conditions. Atmospheric CO_2 concentration is derived from Keeling and Whorf (2005) and N deposition data is taken from Lamarque *et al* (2011). Land use is taken into account with cropland and pastures being treated as natural grasslands, which is a standard simplified representation of managed land-use without additional processes such as harvest or grazing (Pugh *et al* 2015). The fractional cover of land use is obtained from Hurtt *et al* (2011).

2.2. Empirical datasets

We compare simulated GPP to the flux tower-based global estimation of GPP from Jung *et al* (2011) and Jung *et al* (2017) (herein after, FLUXCOM) and the EO-based MODIS (Moderate-resolution Imaging Spectroradiometer) GPP product (MOD17 v55) from (NTSG 2015), at global scale during 2000–2009. These 10 years mark the temporal common time period of the datasets used in table 1. The FLUXCOM here includes four GPP products derived from different machine learning methods: model trees ensemble (MTE, Jung *et al* 2009), Artificial Neural Networks (ANN, Papale and Valentini 2003), Multivariate Adaptive Regression Splines (MARS, Friedman 1991) and Random Forests (RF, Breiman 2001).

2.3. Land cover classes

The land cover classification (figure 1) is used to aggregate the global land area into six land cover categories: tropical forest, extra-tropical forest (boreal and temperate), semi-arid ecosystems, tundra and arctic shrub land, grasslands and land under agriculture (crops, here combined), and areas classified as barren (sparsely vegetated). This classification is based on the MODIS land cover classification, MCD12C1 type3 (Friedl *et al* 2002) and the Köppen-Geiger climate classification system (Kottek *et al* 2006) following Ahlström *et al* (2015).

2.4. Partitioning of climate induced uncertainty

We partition climate induced uncertainty in simulated GPP into temperature, precipitation and shortwave radiation. Six climate datasets are available in this study, which limits our ability to partition uncertainties to specific climatic drivers. Therefore, we combine climate variables of the different datasets in such a way that a given simulation can be forced by the temperature from one dataset, the precipitation from another and the radiation from a third dataset. This approach also allows us to investigate the potential maximum GPP uncertainty stemming from climate variables from different climate datasets. The maximum potential climate induced uncertainty is found by first calculating the apparent model

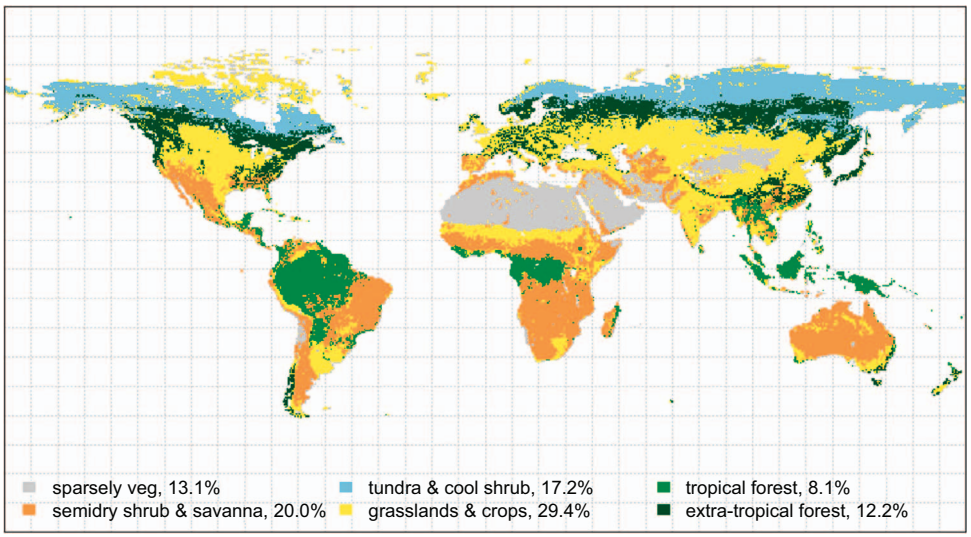

Figure 1. Land cover for aggregating model output for analysis. The percentage values show the fraction of each land cover class of terrestrial area (excluding Greenland).

sensitivities to each of the three climate drivers using multiple linear regressions on an ensemble of simulations where climate variables are combined from a subset ($n = 3$) of the six climate datasets. The maximum potential GPP uncertainty is then found by multiplying the apparent model sensitivities to the climate drivers with the range (maximum minus minimum) of each of the climate drivers at each location (grid cells).

We select three out of six datasets (CRU, NCEP and ECMWF) since their corresponding global GPP represent the minimum, median, and maximum (997, 1064, and 1089 g C m^{-2} yr^{-1}, respectively) within the 6 datasets. We run the simulations with the full combination of these 3 dataset (27 simulations), plus 3 original simulations for the other climate datasets. With these 30 simulation results, we use a multiple linear regression approach to identify the relative importance of each climate variable to total climate induced uncertainty in GPP. The regression is performed separately for each grid cell, cross climate datasets or combinations of climate variable among datasets but not along the time series:

$$\mathrm{GPP} = \alpha \times R + \beta \times P + \gamma \times T + \varepsilon \qquad (1)$$

where GPP, R, P and T represent z-scores (number of standard deviations from the mean) of the annual mean values of GPP, shortwave radiation, precipitation and temperature, respectively, used to force the simulation under consideration. The regression parameters α, β and γ represent the apparent model sensitivities to each of the drivers while ε is the residual error term. We refer to these sensitivities as apparent model sensitivities because they may be influenced by co-variation between climate variables (e.g. Piao *et al* (2013)). To investigate the potential influence of co-variation between the predictors we performed principal components regression (PCR) for analysis of the relationship between GPP and climate. Both analyses yield very similar sensitivities (see supplement 2 and figures S1–4) which add confidence that the sensitivities presented here are good approximations of the model's sensitivities and not heavily influenced by predictor co-variation.

The true sensitivities should ideally also include interaction terms between the variables, and other drivers not explicit in (1), for instance atmospheric CO_2 concentration, may also contribute to the variability of GPP. However, for clarity we choose to illustrate an isolated effect of a driver on the climate induced uncertainty. This is motivated by the fact that interactions only explain a small part (~5%) of the response variability in GPP according to ANOVA analysis (figure S5).

Once the regression coefficients (α, β, γ) are determined, the partial GPP uncertainty caused by the corresponding variables (shortwave radiation, precipitation, temperature) is estimated by:

$$\mathrm{GPP_{R\_unc}} = \alpha \times R_{\_range} \qquad (2)$$

$$\mathrm{GPP_{P\_unc}} = \beta \times \mathrm{P}_{\_range} \qquad (3)$$

$$\mathrm{GPP_{T\_unc}} = \gamma \times \mathrm{T}_{\_range} \qquad (4)$$

$$\mathrm{GPP_{unc}} = \mathrm{GPP_{R\_unc}} + \mathrm{GPP_{P\_unc}} + \mathrm{GPP_{T\_unc}} \qquad (5)$$

where $\mathrm{GPP_{R\_unc}}$ is the partial GPP uncertainty caused by shortwave radiation (2), and α presents an apparent GPP uncertainty sensitivity to shortwave radiation range, $R_{\_range}$, which is the difference between the minimum and maximum shortwave radiation value across forcing datasets. Equations (3) and (4) are analogous cases for precipitation and temperature, and the total GPP uncertainty ($\mathrm{GPP_{unc}}$) is the sum of the three partial GPP uncertainties.

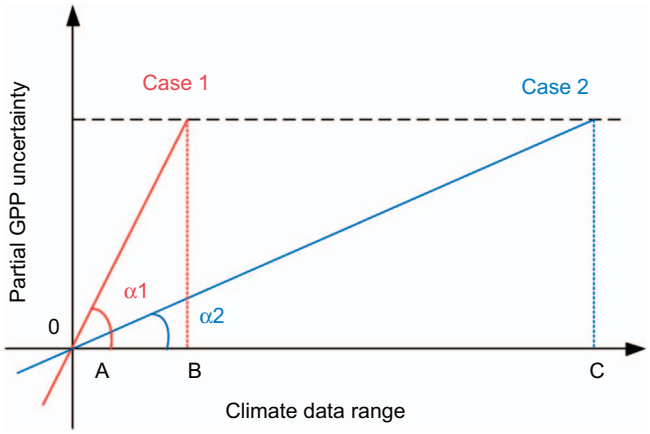

Figure 2. Graphical explanation of how climate data range and apparent model sensitivity contribute to the partial GPP uncertainty. Here shortwave radiation is used as an example. The Y axis represents the partial GPP uncertainty, i.e. the uncertainty caused by shortwave radiation, see equation (2), and the X axis represents the data range of shortwave radiation. The slope of the lines ($\alpha 1$ and $\alpha 2$) represent the change in partial GPP uncertainty for change in shortwave radiation. Both cases have the same GPP uncertainty, caused either by high apparent model sensitivity and small climate data range (AB, red line (case 1)) or by low apparent model sensitivity and large climate data range (AC, blue line (case 2)).

2.5. Partitioning of uncertainty into model sensitivity and climate uncertainty

We also assess how the uncertainty in GPP arises from a combination of climate data uncertainty and apparent model sensitivity by decomposing the partial GPP uncertainty into components associated with the climate data range and simulated apparent sensitivity of ecosystem GPP to the respective driver. Figure 2 shows an example of two possible outcomes with the same partial GPP uncertainty caused by shortwave radiation but with different contributions from climate data range and apparent model sensitivity. For Case 1, apparent model sensitivity contributes more than the climate data range, while the climate data range has higher influence in Case 2. The regression slopes provide their relative contributions to the partial GPP uncertainty (being larger or smaller than 1). Therefore, the fractions of apparent model sensitivity (f_{sen}) and climate data range (f_{range}) that contribute to a climate driver (e.g. shortwave radiation) induced GPP uncertainty can be estimated by:

$$f_{\mathrm{sen}} = \frac{|\alpha|}{|\alpha| + 1} \tag{6}$$

$$f_{\mathrm{range}} = 1 - f_{\mathrm{sen}} \tag{7}$$

where α is the regression coefficient of multiple regression for shortwave radiation, $|\alpha|$ stand for the absolute value of α.

3. Results

3.1. Simulated GPP using six climate datasets

Global GPP simulated by LPJ-GUESS when forced by the six climate datasets without any mixing of climate variables between the datasets shows agreement with FLUXCOM and MODIS GPP (figure 3(*a*)). However, when stratified by land cover classes, the simulated GPP of the tropical forest (figure 3(*e*)), shows markedly lower values than both FLUXCOM and MODIS GPP, while for grasslands, croplands (figure 3 (*d*)) and extra-tropical forest (figure 3(*f*)), simulated GPP is higher than both FLUXCOM and MODIS. These biome-specific discrepancies tend to cancel out to produce a simulated global GPP estimate closer to the remote sensing and flux tower-based estimates (Piao *et al* 2013). Aggregated to the global land surface area, the range among simulations amounts to 11 Pg C yr^{-1} or 9% of mean GPP.

3.2. Climate induced uncertainty—combining climate variables among climate datasets

Here we show inferred apparent model sensitivities (section 3.2.1) and the maximum potential climate induced GPP uncertainty (section 3.2.2) as inferred by applying the regression-based partitioning on an ensemble of ($n = 30$) simulations. The simulations differ only in forcing climate, where climate variables from $n = 3$ climate datasets have been mixed to new and unique combinations. This method allowed us to better investigate the apparent model sensitivity and to investigate the maximum potential climate induced GPP uncertainty. Section 3.2.3 describes the results of partitioning of GPP uncertainty into apparent model sensitivity and climate data range.

3.2.1. Local apparent model sensitivities.

Applying the partitioning method (equations (1–5)) to individual terrestrial locations (grid cells), allows us to generate a global map of the relative importance of the three climate factors in inducing uncertainty in GPP (figure 4). The result shows that precipitation dominates climate induced uncertainty in arid regions and primarily at lower latitudes and cover approximately half (~48%) of the terrestrial vegetated land

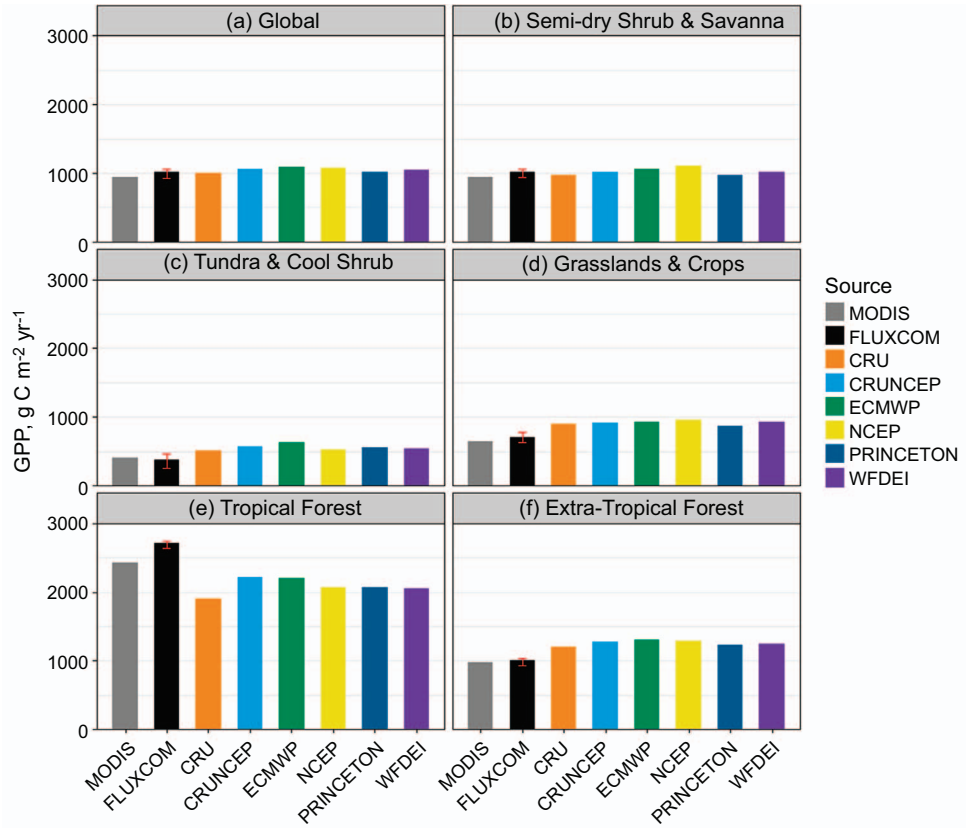

Figure 3. Annual mean GPP during 2000–2009 estimated by LPJ-GUESS forced by the six climate datasets (without combining climate variables), MODIS and FLUXCOM as global totals and stratified by land cover classes (figure 1). FLUXCOM GPP presents the average of the four products (MET, ANN, MARS and RF), and the error bars show the range among these four products (figure S6 shows GPP of individual products). LPJ-GUESS GPP (mean value among simulations, 1048 g C m^{-2} yr^{-1}) is very close to MODIS and FLUXCOM data, while they diverge at regional scale.

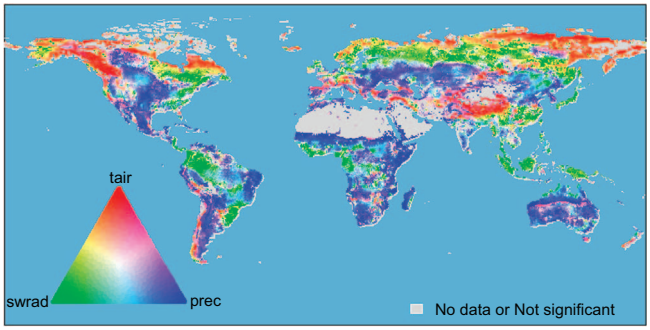

Figure 4. Relative importance of climate factors (red: temperature; blue: precipitation; green: shortwave radiation) to ensemble uncertainty in GPP. Non-vegetative regions and areas with no significant relationship between GPP change and climate change are masked as grey. Precipitation dominates the climate uncertainty over the largest area among the three drivers.

surface. The areas dominated by temperature and shortwave radiation are roughly equal in areal extent and make up the remainder of the terrestrial vegetated surface, with shortwave radiation dominating in moderate to densely wooded ecosystems whereas temperature tends to dominate in high latitude and/or high altitude areas. A similar pattern is found when only using $n = 6$ simulations and not combining climate variables from the different climate datasets, but due to its lower number of data points the regression-based partitioning is statistically less significant (figure S7).

3.2.2. Potential maximum climate induced GPP uncertainty

The potential maximum climate induced uncertainty revealed by the analysis of simulations forced by temperature, precipitation and shortwave radiation data combined from different datasets is shown in figure 5. This result is generated by area weighted average of local GPP uncertainty globally and for each land cover class, and represents the local relative importance of climate drivers (figure 4) averaged over land cover classes. Large differences are apparent among land cover classes in terms of the relative

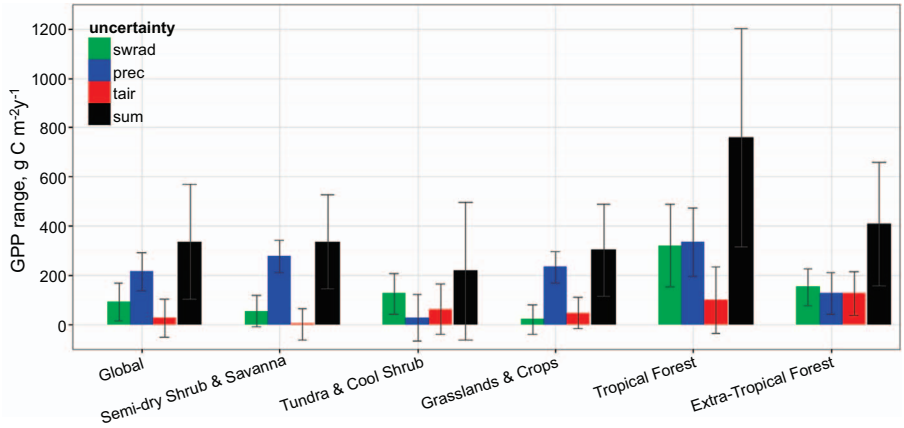

Figure 5. Ensemble GPP uncertainty (black bar) between model simulations calculated from combinations of climate variables among six climate datasets. This result is derived from averaging local GPP uncertainty globally and for each land cover class. Red, blue and green bars show contributions of temperature, precipitation, and shortwave radiation, respectively, to the total climate induced uncertainty in GPP. Error bars show 95% confidence interval. Shortwave radiation and precipitation over tropical forests stand out as large contributors to global GPP uncertainties stemming from differences between climate datasets.

contributions of different drivers to the total uncertainty. Aggregated to the global scale, the potential maximum uncertainty is 41 Pg C yr^{-1} (32% of mean GPP), or nearly four times the uncertainty of 11 Pg C yr^{-1} emerging from simulations based on a single driving dataset (i.e. when not combining climate variables, section 3.1). Error bars show the confidence interval of 95%. Negative values from error bars indicate that we cannot infer that the variable contributes to GPP uncertainties at all at 95% confidence level. The relatively low confidence as indicated by the error bars can partly be explained by small sample size (fewer simulations), inevitable co-variation between climate variables and the stochastic behaviour of LPJ-GUESS. The PCR analysis gives the same result with narrow confidence bands (figure S2). The influence of the stochastic behaviour can also be reduced when using more replicate patches ($n = 20$ here), which reduces the influence of stochastic disturbances (like windstorms or wildfires) on the average of GPP within a grid cell. Another effect of spatial averaging before applying the climate uncertainty partitioning is a decrease of the total uncertainty (16% of mean GPP), which is a result of spatial cancelation of local variation in GPP and climate variables (figures S8 and S9). The climate induced uncertainty is highest for tropical forest and is mainly due to shortwave radiation and precipitation uncertainty followed by air temperature.

3.2.3. Partitioning of GPP uncertainty into apparent model sensitivity and climate data range

The climate induced uncertainty is further partitioned into apparent model sensitivity and climate data range to give an estimate of their relative importance, i.e. do large GPP uncertainties stem from a large sensitivity in the model response to small difference in the drivers, or do the GPP uncertainty arise from low sensitivity in the model response but large difference between the drivers?. Climate data range contributes more to the climate induced uncertainty than apparent model sensitivity to forcing (figure 6). Forested ecosystems show high apparent model sensitivity to shortwave radiation, whereas arid, high latitude and high altitude regions show high apparent model sensitivities to temperature and precipitation. In general, precipitation induced uncertainty has a relatively strong association to apparent model sensitivity in both magnitude and spatial extent, comparing to temperature and shortwave radiation induced uncertainty. Figure 7 shows aggregation of the fractional contributions of apparent model sensitivity and climate data range for each climate variable globally and for each land cover class, via averaging the local fractional contributions (figure 6). Apparent model sensitivity for shortwave radiation causes a slightly higher uncertainty in forested areas compared to other land cover classes. Although precipitation induced uncertainty strongly associated to the precipitation range, the importance of apparent model sensitivity is revealed in dry and tropical ecosystem. The uncertainty induced from temperature is mainly caused by the temperature range among the datasets, while apparent model sensitivity contribution increased in boreal ecosystems.

4. Discussion

This study reveals that differences between global climate datasets induce considerable uncertainty in simulated gross primary productivity in our model. The data uncertainty stems from differences in the data sources and methodology used to construct the climate datasets, and from the sensitivity of the modeled processes to these differences globally and for different climatic regions and land cover classes.

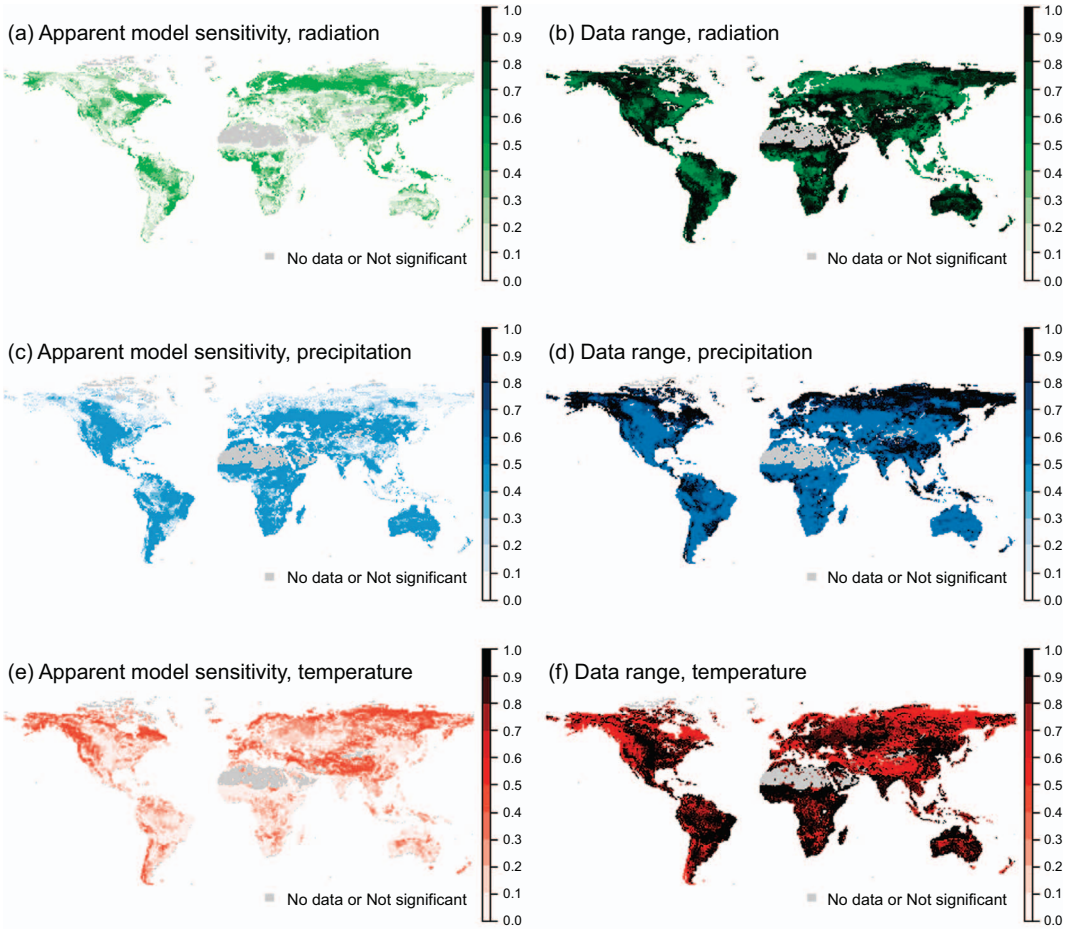

Figure 6. Global distribution of fractional contributions of apparent model sensitivity and climate data range to ensemble climate induced uncertainty for each climatic driver variable. Panels (*a*) and (*b*) show the fraction of contribution of apparent model sensitivity and climate data range to shortwave radiation induced uncertainty (these two fractions sum to 1). Similarly, panels (*c*) and (*d*) are for precipitation, and panels (*e*) and (*f*) are for temperature. Non-vegetative regions and areas without a significant relationship between GPP changes and climate changes are masked as grey. Climate data ranges are found to contribute more to the climate induced uncertainty than apparent model sensitivity to forcing.

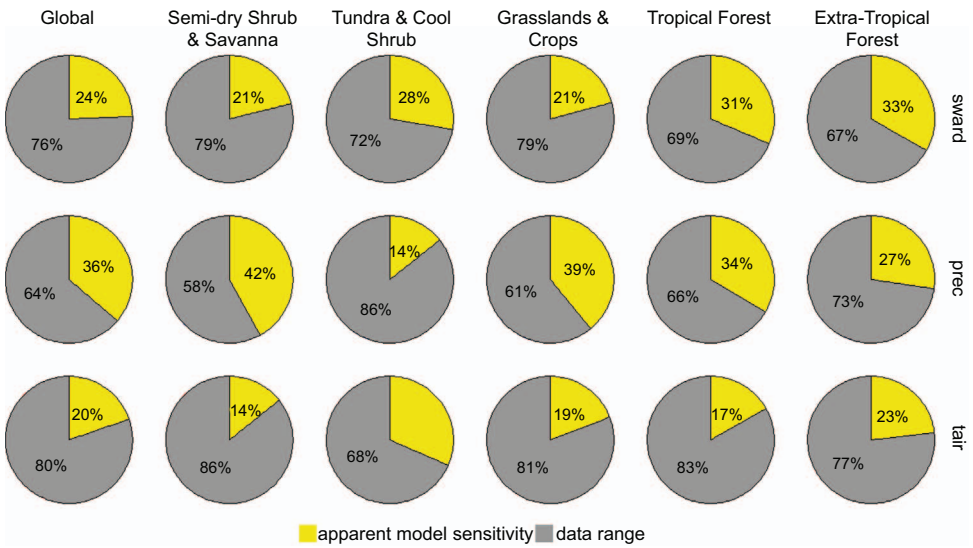

Figure 7. Fractional contributions of apparent model sensitivity and climate data range to ensemble climate induced uncertainty for each climatic driver variable. Climate induced uncertainty are mainly caused by climate data range, whereas apparent model sensitivity is revealed to be relatively important to precipitation induced uncertainty in dry and tropical ecosystem.

4.1. Suitability of the model for this study

By using only a single model (LPJ-GUESS), our analysis excludes quantification of uncertainty stemming from differences in the structure and parameterization of alternative carbon cycle models. However, LPJ-GUESS is a well-established DGVM that has been evaluated and applied in a wide range of published studies, and has also been found to show relatively similar predictive skills and response to climate variations compared to other global ecosystem models (McGuire *et al* 2012, Murray-Tortarolo *et al* 2013, Piao *et al* 2013, Sitch *et al* 2015). Most models simulate similar GPP inter-annual variations at global scale, and these have been traced to large-scale variations in climate, particularly linked to global circulation phenomena such ENSO (Ahlström *et al* 2015). While our study does not address variation among models in sensitivity to climate forcing, we believe that our findings are likely to be representative for global ecosystem models as a class. LPJ-GUESS may thus tentatively be considered representative for how other DGVMs and carbon cycle models behave in response to uncertainties induced by climate forcing data. Although FLUXCOM and MODIS are considered as evaluation data in this study, both datasets involve considerable components of modeling (additionally to the measurement uncertainty) and are therefore also subject to some limitations and uncertainty (Zhao *et al* 2006, Jung *et al* 2011, Lin *et al* 2011). Further, both empirical datasets depend on climate data to extrapolate site measurements to gridded estimates of GPP. Previous studies have evaluated sources of uncertainty in the FLUXCOM (Jung *et al* 2009, Beer *et al* 2010, Jung *et al* 2011), and MODIS GPP products (Running *et al* 2004, Zhao *et al* 2005, Zhao and Running 2010).

4.2. Climate data and climate induced uncertainty

The six climate datasets analysed are derived from either quasi-point-based measurements or climate model-based reanalysis. Station networks, however, vary greatly in density across the globe, with sparse coverage over certain areas, such as the high latitudes (Jones and Harris 2013). Hence the data represent a limited sampling fraction and include an unknown error. Comparing the three main climatic variables of these datasets (figures S10–S12) reveals no strong overall difference in temperature over global and regional scales while a clear difference can be observed for precipitation and shortwave radiation, especially over tropical regions. Our results bring forward that these differences translate into large differences in simulated GPP in our model, and likely in other carbon cycle models.

The potential maximum climate induced uncertainty, if we combine climate variables from different datasets, is found to be 32% of mean GPP. Although the potential maximum uncertainty appears large, Barman *et al* (2014) found that the climate induced uncertainty could reach 20%–30% for simulations of savanna, grassland, and shrubland vegetation types. However, the way the maximum potential uncertainties are calculated here assumes that the most extreme values of each climate variable at each location are compared to create the simulated maximum and minimum GPP. This maximum uncertainty is therefore rather an illustration of the importance of climate drivers and to a lesser extent a representation of actual and realistic uncertainties; in most simulations cancellation effects will reduce the aggregated uncertainties presented here.

The tropical region shows disproportionate large climate induced uncertainty (figure 5) and empirical uncertainty based on observations (figure 3(*e*)). Earlier studies have likewise identified the tropics as a region of high spread in estimated GPP depending on forcing (Zhao *et al* 2006, Poulter *et al* 2011, Ahlström *et al* 2012b, Anav *et al* 2015). Data limitations are likely to be an important source of a high model spread in GPP. Meteorological station networks are generally sparse across the tropics (Medany *et al* 2006). Moreover, characterization of the climate, as based on measurements and modeling, is challenging for tropical regions due e.g. to the influence of extreme climate events (Trewin 2014, Wentz 2015) and the impact of heavy and extended cloudiness on remote sensing measurement (Fensholt *et al* 2007). Furthermore, the results show that the large uncertainty is mainly due to precipitation and radiation, which coincides with findings at site level of Barman *et al* (2014). Jung *et al* (2007) suggested that cloud and aerosol physics (which govern precipitation and radiation transfer) are most likely the principal causes of differences in precipitation and radiation estimates between datasets, since cloud and aerosol properties are implemented differently in different meteorological reanalyses. Our finding as to the global distribution of climate-induced uncertainty in GPP (figure 4) agrees with a recent empirically based study of the sensitivity of global terrestrial ecosystem to climate variables (Seddon *et al* 2016), who found ecologically sensitive regions with amplified responses to climate variability over the world. Moreover, the relative contributions of drivers show similarities in spatial patterns compared to the study by Nemani *et al* (2003) mapping the primary climate constraints to plant growth.

4.3. Apparent model sensitivity and climate data range

Overall, climate data range contributes more uncertainty to simulated global GPP than the sensitivity of the simulated ecosystem processes to climate forcing. This implies that errors in climate datasets play an important role in model-based carbon cycle estimations, and may exceed the importance of shortcomings in ecosystem model structure or parameterisation. We found that GPP uncertainties in simulations by our

model are associated strongly to precipitation in large spatial extent (figure 4). In contrast to the general case described above, precipitation induced uncertainty in dry and tropical ecosystem is also relatively strong associated to apparent model sensitivity to the climate forcing (figures 6(*c*) and (7)). In other words, LPJ-GUESS simulated GPP has a strong sensitivity to precipitation at the global scale, though a model intercomparison study suggests DGVMs in general may be even more sensitive to precipitation than LPJ-GUESS (Piao *et al* 2013). Recent studies emphasize the importance of precipitation variation in controlling vegetation growth, driving inter-annual variability and dominating uncertainty in predictions of future plant production (Beer *et al* 2010, Ahlström *et al* 2012a, Ahlström *et al* 2015).

4.4. Limitations

Aside from limitations, discussed in section 4.1, to the generality of our findings due to the choice of a single (though arguably representative) carbon cycle model, this study is limited by the availability of independent climate datasets. The six climate datasets used here are relatively few to accurately estimate ensemble summary statistics, therefore we decide to combine climate variables of the different datasets to assess the potential maximum climate induced uncertainty. Current (Model Intercomparison Projects) MIPs do use climate forcing that are combinations of other datasets (e.g. Séférian *et al* (2015)), which is valuable to investigate the influence of differences between climate datasets. We apply the multiple linear regression method mainly because the different datasets vary only to a limited extent and therefore the assumption of a linear response of GPP is reasonable. If larger differences between the datasets would have been found in the screening of the data, a non-linear parameterization of the relationship between GPP and the climate variables would have been required (e.g. GPP is positively related to temperature over a certain part of the temperature gradient but too high temperature can cause drought stress). The partitioning between uncertainty stemming from apparent model sensitivity and data uncertainty should therefore be considered indicative and exact numbers are not reported here. Moreover, previous studies (Piao *et al* 2013, Seddon *et al* 2016) have addressed empirically linear relationship between vegetation productivity and climate.

We acknowledge that dependencies between the three climate variables exist, but since we are interested in the response of the model to differences in the climate data we consider these potential inter-dependences as less important for our purpose. Two-way or three-way interactions among climate variables can be substantial for both carbon and water processes. These multiple forcing interactions are not included in this study due to a small contribution to GPP variability (figure S5). It will be a future research challenge to adequately quantify interactive climatic uncertainty and corresponding apparent model sensitivity and interactive climatic data range.

5. Conclusion

We have shown that climate data uncertainties have a large influence on simulated GPP, globally and regionally, and that this uncertainty arises from a combination of differences among driver datasets and the sensitivity of simulated ecosystem processes to climate forcing. Based on our findings, we argue in favour for increased research efforts in constructing historical climate datasets in tropical areas which are found here to be of disproportionate importance for climate uncertainty with potentially large implications for assessments of global carbon cycling and sequestration. Globally and regionally, the choice of climate dataset will continue to affect both empirical data products and model results on the terrestrial carbon cycle.

Acknowledgments

This study is a contribution to the Strategic Research Areas BECC and MERGE, and to the Lund University Centre for Studies of Carbon Cycle and Climate Interactions (LUCCI). We acknowledge Martin Jung for providing FLUXNET GPP data through the site: www.bgc-jena.mpg.de/geodb/projects/Home.php. The work of Veiko Lehsten on this project has been supported by the FORMAS project CONNECT. Anders Ahlström acknowledges support from The Royal Physiographic Society in Lund (Birgit and Hellmuth Hertz' Foundation) and the Swedish Research Council (637-2014-6895).

References

Ahlström A, Miller P A and Smith B 2012a Too early to infer a global NPP decline since 2000 *Geophys. Res. Lett.* **39** L15403

Ahlström A, Raupach M R, Schurgers G, Smith B, Arneth A, Jung M, Reichstein M, Canadell J G, Friedlingstein P and Jain A K 2015 The dominant role of semi-arid ecosystems in the trend and variability of the land CO_2 sink *Science* **348** 895–9

Ahlström A, Schurgers G, Arneth A and Smith B 2012b Robustness and uncertainty in terrestrial ecosystem carbon response to CMIP5 climate change projections *Environ. Res. Lett.* **7** 044008

Ahlström A, Smith B, Lindström J, Rummukainen M and Uvo C 2013 GCM characteristics explain the majority of uncertainty in projected 21st century terrestrial ecosystem carbon balance *Biogeosciences* **10** 1517–28

Anav A, Friedlingstein P, Beer C, Ciais P, Harper A, Jones C, Murray-tortarolo G, Papale D, Parazoo N C and Peylin P 2015 Spatiotemporal patterns of terrestrial gross primary production: a review *Rev. Geophys.* **53** 785–818

Barman R, Jain A K and Liang M 2014 Climate-driven uncertainties in modeling terrestrial gross primary production: a site level to global-scale analysis *Glob. Change Biol.* **20** 1394–411

Battin T J, Luyssaert S, Kaplan L A, Aufdenkampe A K, Richter A and Tranvik L J 2009 The boundless carbon cycle *Nat. Geosci.* **2** 598–600

Beer C, Reichstein M, Tomelleri E, Ciais P, Jung M, Carvalhais N, Rödenbeck C, Arain M A, Baldocchi D and Bonan G B 2010 Terrestrial gross carbon dioxide uptake: global distribution and covariation with climate *Science* **329** 834–8

Breiman L 2001 Random forests *Machine Learning* **45** 5–32

Cox P and Jones C 1993 Illuminating the modern dance of climate and CO *Development* **117** 29

Cramer W, Bondeau A, Woodward F I, Prentice I C, Betts R A, Brovkin V, Cox P M, Fisher V, Foley J A and Friend A D 2001 Global response of terrestrial ecosystem structure and function to CO_2 and climate change: results from six dynamic global vegetation models *Glob. Change Biol.* **7** 357–73

De kauwe M G, Medlyn B E, Zaehle S, Walker A P, Dietze M C, Wang Y P, Luo Y, Jain A K, El-masri B and Hickler T 2014 Where does the carbon go? A model–data intercomparison of vegetation carbon allocation and turnover processes at two temperate forest free-air CO_2 enrichment sites *New Phytolo.* **203** 883–99

Dee D, Uppala S, Simmons A, Berrisford P, Poli P, Kobayashi S, Andrae U, Balmaseda M, Balsamo G and Bauer P 2011 The ERA-Interim reanalysis: configuration and performance of the data assimilation system *Q. J. R. Meteorol. Soc.* **137** 553–97

Farquhar G, Von Caemmerer S V and Berry J 1980 A biochemical model of photosynthetic CO_2 assimilation in leaves of C3 species *Planta* **149** 78–90

Fensholt R, Anyamba A, Stisen S, Sandholt I, Pak E and Small J 2007 Comparisons of compositing period length for vegetation index data from polar-orbiting and geostationary satellites for the cloud-prone region of West Africa *Photogramm. Eng. Remote Sens.* **73** 297–309

Friedl M A, Mciver D K, Hodges J C, Zhang X, Muchoney D, Strahler A H, Woodcock C E, Gopal S, Schneider A and Cooper A 2002 Global land cover mapping from MODIS: algorithms and early results *Remote Sens. Environ.* **83** 287–302

Friedman J H 1991 Multivariate adaptive regression splines *Ann. Stat.* **19** 1–67

Gerten D, Schaphoff S, Haberlandt U, Lucht W and Sitch S 2004 Terrestrial vegetation and water balance—hydrological evaluation of a dynamic global vegetation model *J. Hydrol.* **286** 249–70

Gurney K R, Law R M, Denning A S, Rayner P J, Pak B C, Baker D, Bousquet P, Bruhwiler L, Chen Y H and Ciais P 2004 Transcom 3 inversion intercomparison: model mean results for the estimation of seasonal carbon sources and sinks *Glob. Biogeochem. Cycles* **18** 95–110

Hickler T, Smith B, Prentice I C, Mjöfors K, Miller P, Arneth A and Sykes M T 2008 CO_2 fertilization in temperate FACE experiments not representative of boreal and tropical forests *Glob. Change Biol.* **14** 1531–42

Hurtt G, Chini L P, Frolking S, Betts R, Feddema J, Fischer G, Fisk J, Hibbard K, Houghton R and Janetos A 2011 Harmonization of land-use scenarios for the period 1500–2100: 600 years of global gridded annual land-use transitions, wood harvest, and resulting secondary lands *Clim. Change* **109** 117–61

Jones P and Harris I 2013 University of East Anglia Climatic Research Unit, CRU TS3. 21: Climatic Research Unit (CRU) Time-Series (TS) Version 3.21 of High Resolution Gridded Data of Month-by-month Variation in Climate (Jan. 1901—Dec. 2012). *NCAS British Atmospheric Data Centre*

Jung M, Reichstein M and Bondeau A 2009 Towards global empirical upscaling of FLUXNET eddy covariance observations: validation of a model tree ensemble approach using a biosphere model *Biogeosciences* **6** 2001–13

Jung M, Reichstein M, Margolis H A, Cescatti A, Richardson A D, Arain M A, Arneth A, Bernhofer C, Bonal D and Chen J 2011 Global patterns of land-atmosphere fluxes of carbon dioxide, latent heat, and sensible heat derived from eddy covariance, satellite, and meteorological observations *J. Geophys. Res. Biogeosciences (2005–2012)* **116** 245–55

Jung M, Reichstein M, Schwalm C R, Huntingford C, Sitch S, Ahlström A, Arneth A, Camps-Valls G, Ciais P and Friedlingstein P 2017 Compensatory water effects link yearly global land CO_2 sink changes to temperature *Nature* **541** 516–20

Jung M, Vetter M, Herold M, Churkina G, Reichstein M, Zaehle S, Ciais P, Viovy N, Bondeau A and Chen Y 2007 Uncertainties of modeling gross primary productivity over Europe: a systematic study on the effects of using different drivers and terrestrial biosphere models *Glob. Biogeochem. Cycles* **21** GB4021

Kanamitsu M, Ebisuzaki W, Woollen J, Yang S-K, Hnilo J, Fiorino M and Potter G 2002 NCEP-DOE AMIP-II reanalysis (R-2) *Bull. Am. Meteorol. Soc.* **83** 1631–43

Keeling C and Whorf T 2005 Atmospheric carbon dioxide record from Mauna Loa *Trends: A Compendium of Data on Global Change. Carbon Dioxide Information Analysis Center* (Oak Ridge, TN: Oak Ridge National Laboratory)

Knorr W and Heimann M 2001 Uncertainties in global terrestrial biosphere modeling: 1. A comprehensive sensitivity analysis with a new photosynthesis and energy balance scheme *Glob. Biogeochem. Cycles* **15** 207–25

Kottek M, Grieser J, Beck C, Rudolf B and Rubel F 2006 World map of the Köppen-Geiger climate classification updated *Meteorologische Zeitschrift* **15** 259–63

Lamarque J-F, Kyle G P, Meinshausen M, Riahi K, Smith S J, Van Vuuren D P, Conley A J and Vitt F 2011 Global and regional evolution of short-lived radiatively-active gases and aerosols in the representative concentration pathways *Clim. Change* **109** 191–212

Lin J Pejam M, Chan E, Wofsy S, Gottlieb E, Margolis H and Mccaughey J 2011 Attributing uncertainties in simulated biospheric carbon fluxes to different error sources *Glob. Biogeochem. Cycles* **25** GB2018

Luo Y 2007 Terrestrial carbon-cycle feedback to climate warming *Annu. Rev. Ecol. Evol. Syst.* **38** 683–712

Luo Y, Gerten D, Le Maire G, Parton W J, Weng E, Zhou X, Keough C, Beier C, Ciais P and Cramer W 2008 Modeled interactive effects of precipitation, temperature, and $[CO_2]$ on ecosystem carbon and water dynamics in different climatic zones *Glob. Change Biol.* **14** 1986–99

Luo Y, White L W, Canadell J G, Delucia E H, Ellsworth D S, Finzi A, Lichter J and Schlesinger W H 2003 Sustainability of terrestrial carbon sequestration: a case study in Duke Forest with inversion approach *Glob. Biogeochem. Cycles* **17** 1021

Mcguire A, Christensen T, Hayes D, Heroult A, Euskirchen E, Kimball J, Koven C, Lafleur P, Miller P and Oechel W 2012 An assessment of the carbon balance of Arctic tundra: comparisons among observations, process models, and atmospheric inversions *Biogeosciences* **9** 3185–204

Mcguire A, Sitch S, Clein J, Dargaville R, Esser G, Foley J, Heimann M, Joos F, Kaplan J and Kicklighter D 2001 Carbon balance of the terrestrial biosphere in the twentieth century: analyses of CO_2, climate and land use effects with four process-based ecosystem models *Glob. Biogeochem. Cycles* **15** 183–206

Medany M, Niang-Diop I, Nyong T and Tabo R 2006 *Background paper on Impacts, Vulnerability and Adaptation to Climate Change in Africa* (Ghana: UNFCCC Convention) pp 21–3

Murray-Tortarolo G, Anav A, Friedlingstein P, Sitch S, Piao S, Zhu Z, Poulter B, Zaehle S, Ahlström A and Lomas M 2013 Evaluation of land surface models in reproducing satellite-derived LAI over the high-latitude Northern Hemisphere. part I: uncoupled DGVMs *Remote Sens.* **5** 4819–38

Nemani R R, Keeling C D, Hashimoto H, Jolly W M, Piper S C, Tucker C J, Myneni R B and Running S W 2003 Climate-driven increases in global terrestrial net primary production from 1982 to 1999 *Science* **300** 1560–3

Numerical Terradynamic Simulation Group (NTSG) 2015 The University of Montana, 32 Campus Drive, Missoula, MT 59812, USA (www.ntsg.umt.edu/project/mod17) [8 May 2015]

Papale D and Valentini R 2003 A new assessment of European forests carbon exchanges by eddy fluxes and artificial neural network spatialization *Glob. Change Biol.* **9** 525–35

Parton W, Scurlock J, Ojima D, Gilmanov T, Scholes R, Schimel D S, Kirchner T, Menaut J C, Seastedt T and Garcia moya E 1993 Observations and modeling of biomass and soil organic matter dynamics for the grassland biome worldwide *Glob. Biogeochem. Cycles* **7** 785–809

Peterson T C, Karl T R, Jamason P F, Knight R and Easterling D R 1998 First difference method: maximizing station density for the calculation of long-term global temperature change *J. Geophys. Res. Atmospheres 1984–2012* **103** 25967–74

Piao S, Sitch S, Ciais P, Friedlingstein P, Peylin P, Wang X, AhlstrÖm A, Anav A, Canadell J G and Cong N 2013 Evaluation of terrestrial carbon cycle models for their response to climate variability and to CO_2 trends *Glob. Change Biol.* **19** 2117–32

Poulter B, Frank D, Hodson E and Zimmermann N 2011 Impacts of land cover and climate data selection on understanding terrestrial carbon dynamics and the CO_2 airborne fraction *Biogeosciences* **8** 2027–36

Prentice I C, Bondeau A, Cramer W, Harrison S P, Hickler T, Lucht W, Sitch S, Smith B and Sykes M T 2007 Dynamic global vegetation modeling: quantifying terrestrial ecosystem responses to large-scale environmental change *Terrestrial Ecosystems in a Changing World* (Berlin: Springer) pp 175–92

Pugh T, Arneth A, Olin S, Ahlström A, Bayer A, Goldewijk K K, Lindeskog M and Schurgers G 2015 Simulated carbon emissions from land-use change are substantially enhanced by accounting for agricultural management *Environ. Res. Lett.* **10** 124008

Running S W, Nemani R R, Heinsch F A, Zhao M, Reeves M and Hashimoto H 2004 A continuous satellite-derived measure of global terrestrial primary production *Bioscience* **54** 547–60

Scheiter S, Langan L and Higgins S I 2013 Next-generation dynamic global vegetation models: learning from community ecology *New Phytolo.* **198** 957–69

Scholze M, Knorr W, Arnell N W and Prentice I C 2006 A climate-change risk analysis for world ecosystems *Proc. Natl Acad. Sci.* **103** 13116–20

Seddon A W, Macias-Fauria M, Long P R, Benz D and Willis K J 2016 Sensitivity of global terrestrial ecosystems to climate variability *Nature* **531** 229–32

Séférian R, Gehlen M, Bopp L, Resplandy L, Orr J C Marti M, Dunne J P, Christian J R, Doney S C and Ilyina T 2015 Inconsistent strategies to spin up models in CMIP5: implications for ocean biogeochemical model performance assessment *Geosci. Model Dev. Discuss.* **8** 8751–8808

Sheffield J, Goteti G and Wood E F 2006 Development of a 50 year high-resolution global dataset of meteorological forcings for land surface modeling *J. Clim.* **19** 3088–111

Sitch S, Friedlingstein P, Gruber N, Jones S, Murray-Tortarolo G, Ahlstörm A, Doney S C, Graven H, Heinze C and Huntingford C 2015 Recent trends and drivers of regional sources and sinks of carbon dioxide *Biogeosciences* **12** 653–79

Sitch S, Huntingford C, Gedney N, Levy P, Lomas M, Piao S, Betts R, Ciais P, Cox P and Friedlingstein P 2008 Evaluation of the terrestrial carbon cycle, future plant geography and climate-carbon cycle feedbacks using five dynamic global vegetation models (DGVMs) *Glob. Change Biol.* **14** 2015–39

Smith B, Prentice I C and Sykes M T 2001 Representation of vegetation dynamics in the modelling of terrestrial ecosystems: comparing two contrasting approaches within European climate space *Glob. Ecol. Biogeogr.* **10** 621–37

Smith B, Warlind D, Arneth A, Hickler T, Leadley P, Siltberg J and Zaehle S 2014 Implications of incorporating *N* cycling and *N* limitations on primary production in an individual-based dynamic vegetation model *Biogeosciences* **11** 2027–54

Tebaldi C and Knutti R 2007 The use of the multi-model ensemble in probabilistic climate projections *Philos. Trans. R. Soc. Lond.* A **365** 2053–75

Trewin B 2014 The climates of the tropics and how they are changing *State of the Tropics* vol 1, pp 39–52

Weedon G, Gomes S, Viterbo P, Shuttleworth W, Blyth E, Österle H, Adam J, Bellouin N, Boucher O and Best M 2011 Creation of the WATCH forcing data and its use to assess global and regional reference crop evaporation over land during the twentieth century *J. Hydrometeorol.* **12** 823–48

Wei Y, Liu S, Huntzinger D, Michalak A, Viovy N, Post W, Schwalm C, Schaefer K, Jacobson A and Lu C 2013 The North American carbon program multi-scale synthesis and terrestrial model intercomparison project–part 2: environmental driver data *Geosci. Model Dev. Discuss.* **6** 5375–422

Wentz F J 2015 A 17-yr climate record of environmental parameters derived from the tropical rainfall measuring mission (TRMM) microwave imager *J. Clim.* **28** 6882–902

Wramneby A, Smith B, Zaehle S and Sykes M T 2008 Parameter uncertainties in the modelling of vegetation dynamics—effects on tree community structure and ecosystem functioning in European forest biomes *Ecol. Model.* **216** 277–90

Zaehle S, Medlyn B E, De Kauwe M G, Walker A P, Dietze M C, Hickler T, Luo Y, Wang Y P, El-Masri B and Thornton P 2014 Evaluation of 11 terrestrial carbon–nitrogen cycle models against observations from two temperate free-air CO_2 enrichment studies *New Phytolo.* **202** 803–22

Zaehle S, Sitch S, Smith B and Hatterman F 2005 Effects of parameter uncertainties on the modeling of terrestrial biosphere dynamics *Glob. Biogeochem. Cycles* **19** 2307–27

Zhao M, Heinsch F A, Nemani R R and Running S W 2005 Improvements of the MODIS terrestrial gross and net primary production global data set *Remote Sens. Environ.* **95** 164–76

Zhao M and Running S W 2010 Drought-induced reduction in global terrestrial net primary production from 2000 through 2009 *Science* **329** 940–3

Zhao M, Running S W and Nemani R R 2006 Sensitivity of Moderate Resolution Imaging Spectroradiometer (MODIS) terrestrial primary production to the accuracy of meteorological reanalyses *J. Geophys. Res. Biogeosciences (2005–2012)* **111** 338–56

Zhou X, Weng E and Lou Y 2008 Modeling patterns of nonlinearity in ecosystem responses to temperature, CO_2, and precipitation changes *Ecol. Appl.* **18** 453–66